Mechanical properties of polymer spliced nanoparticle composites

Afreen Begum

Assistant professor at Shahdan women's college of Engineer and technology. Khairtabad, Hyderabad, Telangana State, India.

afreen.mech302@gmail.com

Abstract

Polymer nano composites have enhanced mechanical, photosensitive and thermal properties related to old-style thermoplastics. To work theresult of spliced brush/broom–matrix connection on the properties of nanoparticles full polymers, uniaxial elastic checking with (DIC-digital image correlation) was done on polystyrene (PS) spliced SiO2 in less molecular weight (MW) (N P), N ¼ degrees of polymerization of spliced brush/broom, P ¼ degrees of polymerization of matrix, and higher MW (2N ¼ P) matrices at unlike loading. The less matrix MW composites had more power than high MW composites at more loading but lesser power than the pure matrix. The higher matrix MW composites have very highdurability at low-slung loadings. SEM image of crack surface revealed plastic and particle debondinginvalidgrowth in the high durability samples. The result shows the ratio P/N ofmechanical properties ofpolymer spliced nanoparticle composites is significant for adapting the properties of polymer spliced nanocomposites.

KEYWORDS toughening; Nanocomposite; mechanical properties; polymer matrix;particle debonding; spliced brush; RAFT polymerization; plastic void growth.

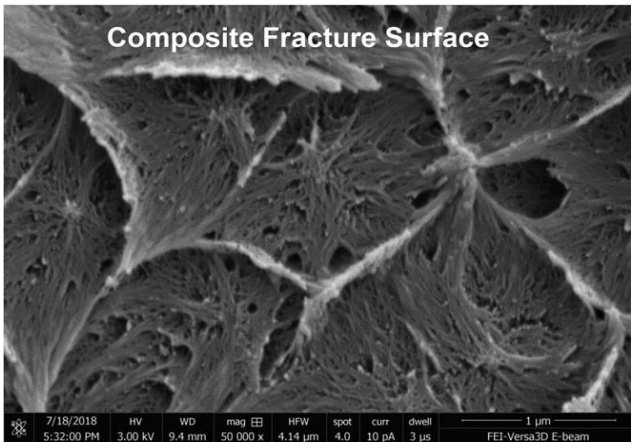

1. Introduction

Polymernanocomposites frequentlyshowbetter mechanical properties, [1–4] optical properties, [5, 6]thermal stability[7–9] and electrical properties[10–12] above their polymer counterparts. The filler size, dispersion and distribution can modify every properties significantly.[13–16] It has been shown that for low-slung filler loadings, composites with well dispersed fillers are utmostprobable to showimproved proper- ties.[17] For example, in fine dispersed 40 nm alumina filled PMMA, rises of an order of magnitude in fracture strain were detected.[18] While for clustered composites with 40 nm Al2O3 and 90 nm Fe3O4 in PMMA and PS,[19] the modulus of the composites was somewhatinferior than clean polymer in all composites measured, which is opposed to what is expected by filler strengthening theories.[20,21]Short molecule changes can lead to betterdispersal, and presentseveral example of fine disperse nanoparticle cumulate the modulus.[20,21] It is also typical that there is an optimal loading to attain the maximum toughness oreffect energy. For example, in 16 nm diameter chlorosilane changed particles in polystyrene, [22]the modulus enlarged with SiO_2 loading. The highest toughness, effect energy and fracture strain were found at 0.75 wt% SiO_2 and SEM images shown some signal of particle debonding.To additional progress dispersion, spliced polymer chains have been used. A bimodal population of brushes/ broom (one group is heavily spliced small brush broomand the other is sparsely spliced long brush) have been found to be optimum for regulating dispersion.[17,23,24]At low-slung loadings, bimodal example have the major modulus in together compression and tension related to monomodal brush changed particles. In detail the bimodal examples have toughness even higher than expected by the GuthGold[20]or HalpinTsai[21]expectations.The interface betweenspliced brush and Matrix polymer is also significant in decisive properties. In examples without any matrix added, the hardest examples had the highest brush molecular weight (and the most entanglements).[25]Not surprisingly, in samples with matrix added, the largest strain to failure was also for samples withthe greatest degrees of entanglement. These experimental observations are supported by computational work. Self-consistent field theory (SCFT) has shown that when the matrix and particles are in the wetting regime, the matrix chains penetrate the grafted corona. To quantify wettability, the interfacial tension of matrix and grafted brush, cb/h, was used.[28] It was found that cb/h > 0 for all P.The utmost degree of predicament. These experimental observations are helped by computational work. Self reliable fields theoretically (SCFT) has displays that when the matrix and particles are in the dampening system, the matrix chains infiltrate the spliced corona.To enumerate wettability, the interfacial pressure of matrix and spliced brush, cb/h, was used.[28] It was originate that cb/h > 0 for all P (degree of polymerization of matrix)>N (degree of polymerization of spliced chain) ratios, however for P < N, cb/h was too lesser to causefilm dewetting. To more understand that contact, the penetration width, w, of the splicedchain has also set on computationally. Matrix infiltration into the brush/brooms is biggest for brushes with animplantthickness in the semi-dilute regime. And as P/N rises, w decreases.[29] Further, if the brush/broom- matrix interactions are revolting,[30] interaction decreases and leads to inferior yield strength than pure matrix. For attractive filler-matrix interactions, computation expects that the yield strength will be the same as the matrix. For spliced chains, higher than 5 Me the fadunsuccessful mechanism is

expectedto be bond breaking, whereas for matrix chain which have low tension (meanwhiletogether ends aren't fixed) the transition to bond breaking happensat 20 Me.These experimental and computational works suggest that the fracture conduct of polymer nanocomposites depends on the brush–matrix interactions which are regulate by the molecular weight and implant density of the brush. The contestresearch has been that it is tough to distinctlymodify the matrix-brush interaction for animmovable dispersion. Bimodal spliced brushespermitliberatedchange of the interaction while keeping good dispersion. Thus, we have developed materials systems of bimodal polystyrene spliced SiO_2 nanoparticles dispersed in polystyrene. The binary sets of composites have *P*/*N* ratios of 1 and 2. We discovery that at specific *P*/*N* ratios and loadings, the mechanical properties are changedaffectinginsignificantlyimprovedstraintofailure.

2. Experimental

2.1. SiO_2 8k 110ksynthesis

Bimodal brush particles were synthesized by means of a sequential changeable additional disintegration chain transmission (RAFT) polymerization related to a procedure described earlier.[17] To a solution of colloidal silica particles (Nissan Chemicals Inc., 30 wt% dispersion in MIBK, SiO2 density = 2.2g/mL) diluted with THF, added 3-amino propyldimethylethoxysilane and a trace volume of octyldimethylmethoxysilane to keep dispersefrom side to side this synthetic step. This combination was warmth at 65°C for 4h beneath an inert (N2) atmosphere. The surface fastened amine group is present then reacted with 2-mercaptothiazoline activated 4-cyanopentanoic acid dithiobenzoate (CPDB). The spliced density of these covalently bound chain transfer agents was resolute by relating a UV–Vis spectrum of a spliced particle examplediscrete in THF to a calibration curve built from recognized amount of free CPDB in solution. The exterior polymerization of styrene monomer was done at 65°C. The polystyrene spliced particles were caused in hexane and improved by centrifugation. The chains from a small sample of polystyrene spliced particles were cleaved using hydrofluoric acid (HF), and the chain length and dispersity were examined by gel-permeation chromatography (GPC). The rest of the sample was discrete in THF. A large additional of azobis (isobutyronitrile) (AIBN) was used to cleave the RAFT agent to stop additional chain growth. The particles, which spliced with the small brush/broom of polystyrene, were refunctionalized with CPDB as definedbeyond. The implant density of the anotherpopulace of chainstransmission agent was determined by standardizing the % silica in the sample based on TGA weight loss due to spliced polystyrene, and this right mass was interrelated with the UV–Vis spectrum of the sample to determine the density of RAFT agents on the silica surface. The polymerization of this anotherpopulace of polystyrene chains was lead as defined above. Afterward the polystyrenespliced particles were hastened in hexane, a lesserexample was taken and the chain cleaved with HF. The molecular weightiness and discrepancy of togetherpopulaces of cleaved chain was examined by GPC. The bimodal polymer spliced particles were redisposed in THF, and the second population of RAFT agent was cleaved using a large excess of AIBN before further use. The bimodal polystyrene spliced SiO2 is stated to as $SiO_2$8k 110k in this

study. Two populaces of polymer brushes/broom were spliced to the exterior: a small polystyrene brush/broom with MW = 8 kg/mol and animplant density = 0.25 chains/nm2 and lengthy polystyrene brush/broom with MW = 110 kg/mol and animplant density = 0.07 chains/nm^2.

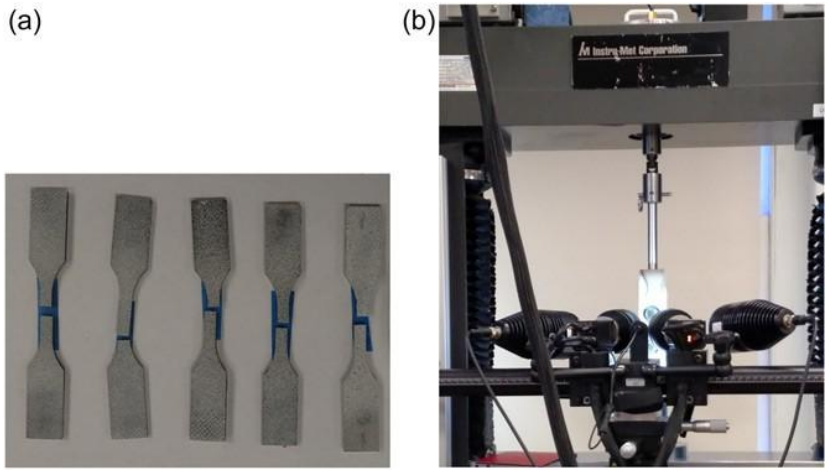

Fig 1. Tensile testing with DIC. (a) Samples after test with speckle pattern and (b) tensile testing load frame, grips and cameras.

2.2 SiO_2–PScomposites

SiO_2 8k 110k in THF was solution mixed with homopolymer matrix (MW = 100 kg/mol or MW =200 kg/mol, from Polymer Source). The samples were mixed with a probe sonicator (Sonics and Materials Vibracell VCX 750 W unit) for 1 min at 40% amplitude using the pulsed setting of 2s on and 0.5 s off. The samples were solution cast into aluminum boats at 90°C.Composites were annealed for 2 days at 120 °C in a vacuum oven. Sample were warm pressed at 190°C andslowlycool.

2.3 TEM-Transmission electron microscopy

Composite samples were entrenched in epoxy. Samples were cut into 60 nm piece by use of an RMC PowerTome XL microtome. The section were floated onto water and transferred to copper grid. The unit was imaged using a JEOL 2011 TEM atago accelerating power voltage of 200 kV. The imagewastransformed to two format using program Image. For each composite[30] images were taken andbinaries. To measure cluster size an algorithm developed by the Brinson and Chen group wasused.[31–33]

2.4 DSC -Differential scanning calorimeter

Composite sample were weight into aluminum pans for purpose of glass changing temperature(T_g). The sample and an empty reference pan wereloadedintoaDSC-

Q100.Theexamplechamber was full with N_2 (g). Composites were heat at 10 °C/min to 160 °C and cooled to 50 °C at aamount of10°C/min.Threeheatandcoolcyclewere run. The glass changing temperature (T_g) was taken as the modulationopinion of thestep.

2.5 TGA-Thermal gravimetric analysis

For SiO_2–PS composites, a TGA-Q50 was used to regulate the filler loading. The samples were loaded into an alumina crucible. The samples chamber was filled with N_2 (g). The samples were warmthfrom25 to800°Catadegreeof20°C/min.

2.6 DIC-Tensiletestingwithdigitalimage correlation

Eight dissimilar sample were made: PS matrix 100k, PS matrix 200k, 0.7 vol.% SiO_2 in 100k PS, 1.3 vol.%SiO_2in100kPS,5.5vol.%SiO_2in100kPS,0.5 vol.% SiO_2 in 200k PS, 1.3 vol.% SiO_2 in 200k PS, and 5.5 vol.% SiO_2 in 200k PS. For every samples 5 specimen were made. Sample was hot pushedat 190 °C by means of a Carver hot press into dog bone sample with dimensions stated by ASTMD638 typeV. The PS and SiO_2–PS composites were ready for 3D DIC measurements by applying a random speckle pattern.[34]The pattern was applied in two steps: first a unchanging white base coat (white enamel paint (Model Master FS37875) with some air brush thinner) was spray painted. Next a random black speckle pattern (Model Master FS37038) was applied. The sample and setup are shown inFig 1. Samples were tested in uniaxial tension using an electro-mechanical load frame (load cell capacity1kN)atroomtemperature.Apreloadof5

Table 1. Materials system for bulk mechanical testing of PS grafted SiO2 in homopolymer PS

sample ID	Matrix MW (kg/mol)	SiO2 loading	Surface modification
100k PS	100	–	–
100k_0.7	100	0.8vol%	PS: 8 kg/mol, 0.25 chains/nm2 PS: 110 kg/mol, 0.07 chains/nm2
100k_1.3	100	1.2vol%	PS: 8 kg/mol, 0.25 chains/nm2 PS: 110 kg/mol, 0.07 chains/nm2
100k_5.5	100	5.6vol%	PS: 8 kg/mol, 0.25 chains/nm2 PS: 110 kg/mol, 0.07 chains/nm2
200k PS	200	–	–
200k_0.5	200	0.4vol%	PS: 8 kg/mol, 0.25 chains/nm2 PS: 110 kg/mol, 0.07 chains/nm2
200k_1.3	200	1.2vol%	PS: 8 kg/mol, 0.25 chains/nm2 PS: 110 kg/mol, 0.07 chains/nm2
200k_5.5	200	5.6vol%	PS: 8 kg/mol, 0.25 chains/nm2 PS: 110 kg/mol, 0.07 chains/nm2

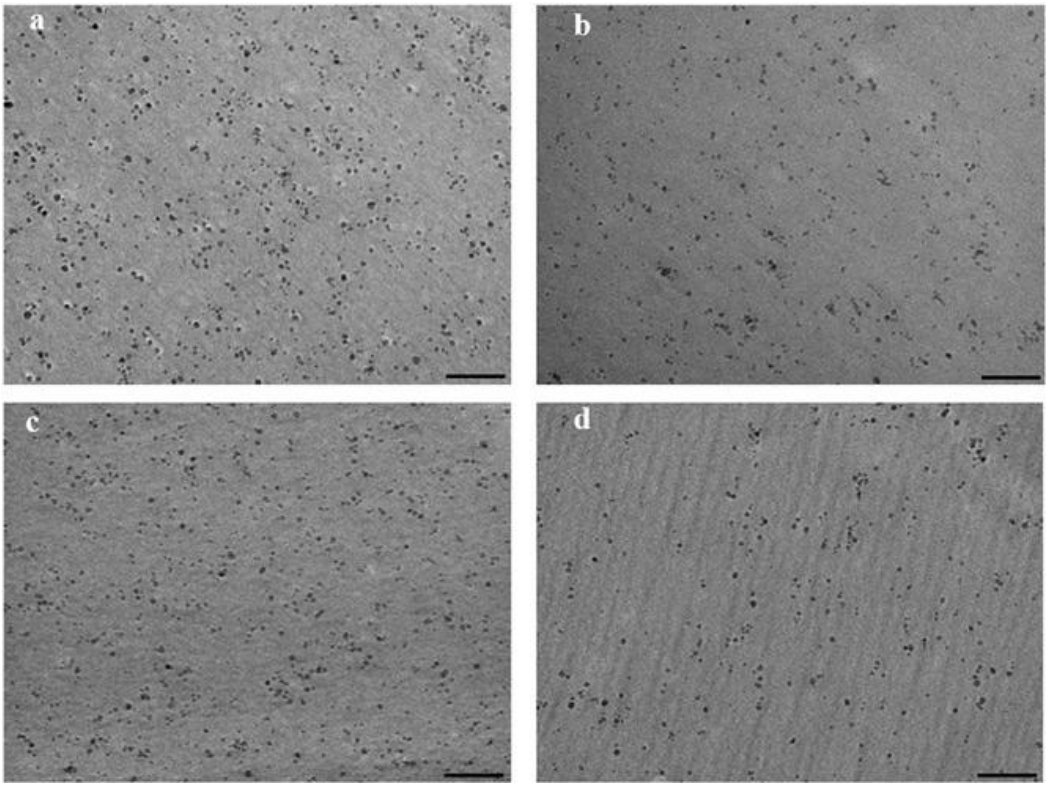

Fig 2. TEM images of SiO2-PS composites, all scale bars 200 nm. (a) Image of 100k_1.3, (b) Image of 100k_0.7, (c) Image of 200k_1.3, and (d) Image of 200k_0.5.

N–7 N was applying to every singlesample. The samples were strained at a straining rate of 1 mm/min. Thestandardized field of sight was 15 mm width × 10 mm height × 5 mm depth of field. Image wastakenby usingcameras 2CCD(2448×2050pixelresolution) withSchneiderUNIFOC2.8/50lenses.Theloadedinformation wastakenfromtheloadcell.TheARAMISsoftware byGOMwasusedtocomparetheimageandcompute strains. Virtual extensometers were positioned on image to compute strain. A virtual extensometer almost7mminlengthwithaaccuracyof 0.001 mm was used to compute axial strain.

2.7 Scanning electron microscopy(SEM) Fractography

The SiO_2–PS composites and PS matrices afterwardtensile testing were well-preserved. The fracture exteriors were splutter covered with 60% Au/40% Pd using a Hummer V sputter coater. The metal layer was 0.5 nm thick. Sample was then image with FEI Versa 3D Dual Beam SEM at accelerating power voltages of 3 kV.

3 Results anddiscussion

The materials system information is displays Table 1. The polymer spliced nanoparticles in 100k PS are forecast to have matrix perception into the splicedbrushsince$N\sim P$,howeverthesplicedchain in 200k PS are predictable to have additional collapsedchain or a less significant quantity of matrix penetration

meanwhile $N < P$.[28,29] To assess the dispersal state of SiO_2–PS composites, TEM was used. The images were binarized and 30 images were taken per composite. An algorithm was apply to the binarized image to removeaverage cluster radius (R_c).[31–33]Illustrative TEM images for the SiO_2–PS composites are display in Fig 2. All images noticeably show that the particles are individually dispersed and well dispersedthrough the micrograph. To quantify the dispersion, $R_c$for each sample was calculated. For each composite sample, R_c=7 nm as expected for finedistributed polymer nanocomposites with 14 nm diameter particles. Thus, any changes in properties cannot be attributed to the particledistribution. The thermal state of polymer nanocomposites is also important when considering the mechanical properties. Specifically, for amorphous polymers the T_g is very important. The T_g values are shown in Table 2below. The 100k PS composites and matrix T_g values are within error of each other. The thermal state doesn't change with particle loading for 100k sample. For the 200k composites, the biggestdifference is less than 2 degrees. Thus, any importantchange in mechanical properties is not due to changes inT_g.Fig 3show the modulus data vs filler volume fraction data (the core SiO_2 volumefraction).The prediction from filler reinforcement theory by Guth–Gold is shown for comparison.[20] the 100k and 200k composites have very similar values formodulus at constant loading and follow the Guth–Gold prediction closely. There are a few deviations from Guth–Gold at very low and high loadings.The strength data vs core SiO2 volume fraction is shown in Fig 3b. The strength of the 100k MW matrix composites does not change significantly with loading, while the 200k matrix composites show a decrease in strength at higher loading. The 100k_0.7 composite failed mostly external the gauge section so the data point is from only 2 specimens. Clearly in these systems, the impact of the matrix– brush interaction is not large enough to change the maximum load significantly at low loadings. At higher loadings, when the brushes have the potential to overlap, the strength begins to decrease. A plot of the inter particle distance is shown in Fig 4. Here inter particle distance, dc–c, includes the core SiO2 particle and the grafted brush. The grafted brush height was calculated as radius of gyration of the long brush (h = 9.1 nm). This has been shown to be a good approximation of brush height according to SAXS and SANS measurements.35 It is clear from Fig 4 that at a high particle loading the interparticle distance is very small. This small distance is likely the cause of the strength decrease. The failure strain data as a function of SiO2 volume fraction is shown in Fig 3c. There is one

Table 2. The Tg for polystyrene matrices and SiO2-PS com- posites. The composites are labeled with vol. % of SiO2 only.

Sample name	Tg (○C)	Sample name	Tg (○C)
100k PS	105.7	200k PS	107.3
100k_0.7	105	200k_0.6	106.9
100k_1.3	106.2	200k_1.2	107.8
100k_5.5	105.3	200k_5.4	105.4

Amazing statistical point. For the 200k_0.5 composite there is a very large strain to letdown. This is the same loading where the reduction in modulus was seen. 100k composites at the

same loadinginclined to fail in the grips, but the little sample tested did not show the rise in strain to failure. The great failure strain and high strength suggest that the 200k_0.5 composite is tougher than all the other samples. Strain energy density, the area under the stress–strain curve, was used as a measure of toughness. The 200k_0.5 composites had twice the strain energy density compared to the matrix. One possible reason for this increased strain energydensity is remaining solvent. Remaining solvent can act as a plasticizer and toughener.[36]All sample was managed in the similar way so it is extremely doubtful that the 200k_0.5 composite has residual solvent. Moreover, if there was residual solvent a decrease in T_g would be seen. In Table 2, the T_g of 200k_0.5 is like to all other samples. To better apprehend this large strain energy density, the fracture surfaces oftensiletestingsampleswereimagedwithSEM. Thefracturesidesofthe200kSiO_2–PScomposites were imaged with SEM and are shown in Figure 5. Representative images for small and big magnification are shown for each sample. The low magnification images for each 200k sample are very similar. The high magnification images have significant differences. In Fig 5b the matrix high magnification image is shown for reference, the fracture surface is very smooth with minimal features. The great magnification image for the 200k_1.3 and 200k_5.5 composites are very parallel to each other and somewhat dissimilar than the matrix image (Fig 5f and h). The SEM images for 200k_1.3 and 200k_5.5 have some small pores which could be from particle debonding. The normal hole size for Fig5fis46nmdiametersandforFig5hitis 41 nm diameter. These voids are roughly 3 times

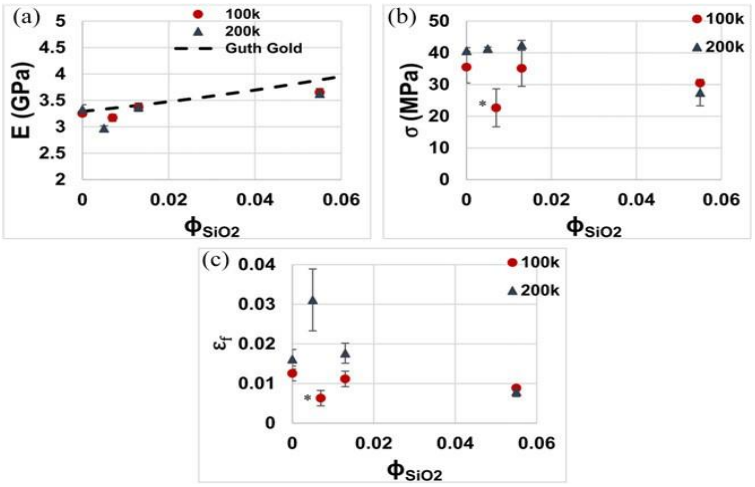

Fig 3. Bulk mechanical properties data for polymer Nano composites. Data points with asterisk only had 2 samples break in gauge length. (a) Modulus vs. Particle loading for polymer Nano composites, (b) Failure strength vs. Particle loading for polymer composites, and (c) failure strain vs. Particle loading for polymer Nano composites. Greater than the SiO2 diameter. The SEM image for 200k_0.5 have very big pores (Fig 5d), much larger than the particle size, 2R = 14 nm, likely there was particle debonding followed by plastic void growth. If we look extra closely at the fracture surface of composite 200k_0.5 we note that there are two regions (Fig 6). There are more voids and larger voids in region 1 than region 2. Region 1 appears to have a

rough fracture surface with a large amount of deformation. Region 1 is likely the slow crack growth region,

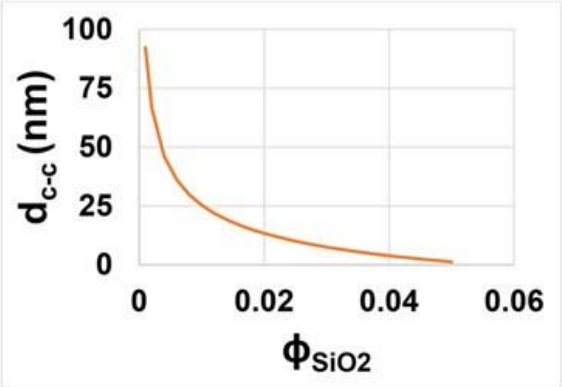

Fig 4. Interparticle distance vs particle loading. The particle is defined as core inorganic SiO2 and grafted PS brush. providing more time for void growth, and region 2 is the fast crack growthregion. To more comprehend the large fracture strain observed for composite 200k_0.5 several toughening mechanisms were considered. Mutual toughening mechanisms for particle filled composites are: crack pinning, crack deflection, shear banding and plastic void growth.[37–40] In crack pinning the particles act as obstacles that the crack will bow around. The crack bowing increases the crack length, which, increases toughness. Our obstacles are 14 nm SiO_2 nanoparticles. In maximum cases of crack pinning the obstacles were greater than the crack tip opening displacement: [41–44]

$$d_{tc} \approx \frac{K_{1c}^2}{E r_y} \delta_1 - t^{2p} \quad (1)$$

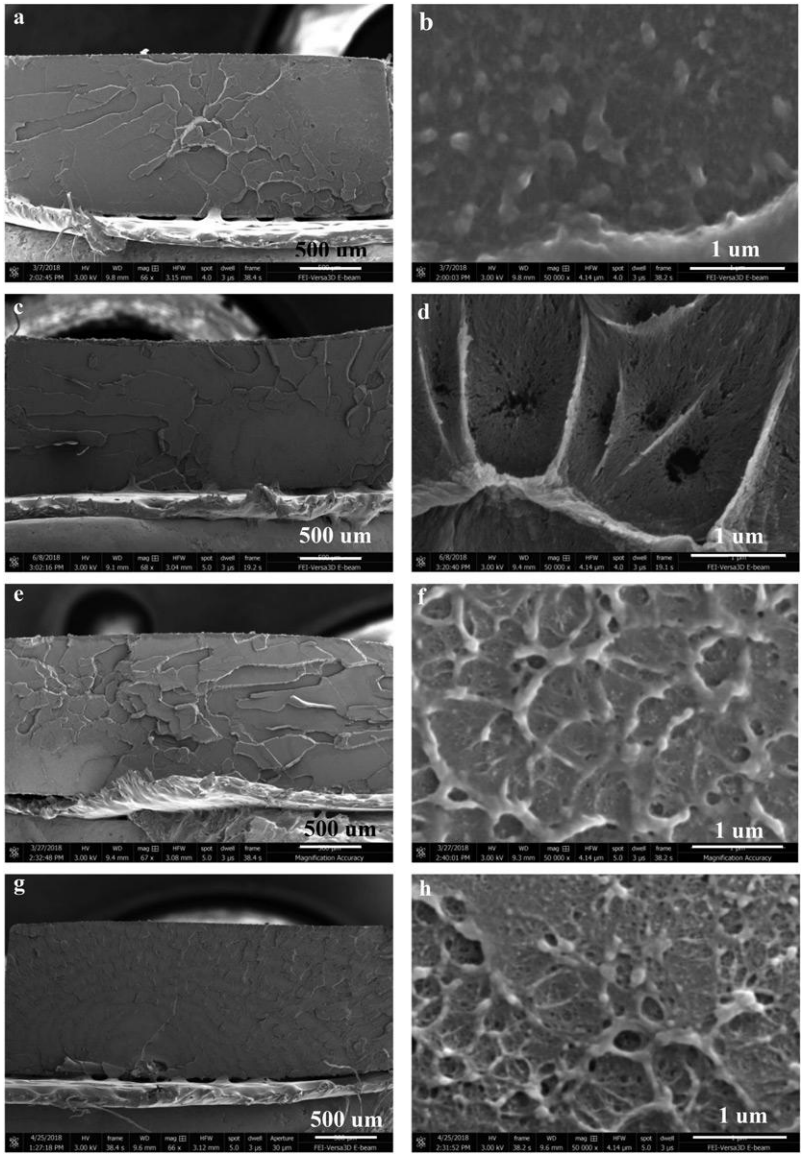

Fig5. SEM images of fractured surfaces (a–b) Images of 200k PS, (c–d) Images of 200k_0.5, (e–f) Images of 200k_1.3, and (g–h) Images of 200k_5.5.

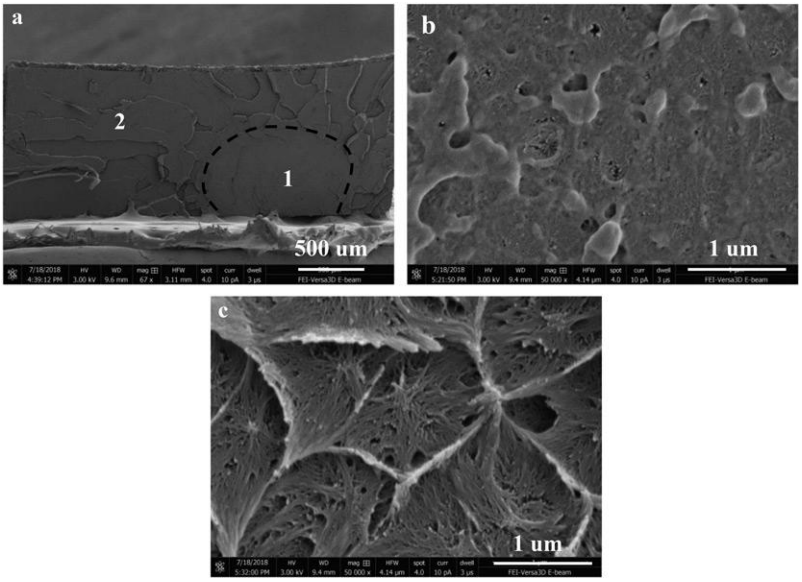

Fig 6. SEM images of fracture surface for composite 200k_0.5. (a) Low magnification image of fracture surface with region 1 and 2 labeled, (b) high magnification image of region 2, and (c) high magnification image of region 1.

Table 3 Properties used in evaluation of toughen- ing mechanisms.

Property		Reference	Property	References	
E	3.14 GPa	–	lm	0.25	47
u	0.33	–	Kvm	2.22	37
ry	41.9	–	ryc	70 MPa	48
K1c	MPapffiffiffiffi	47	ry	24.5 um	–

The – in reference column indicates it was measured experimentally.

Where dtc is crack opening displacement, K_{1c} is stress and u is Poisson's ratio. Using the values in Table 3, dtc =6.1 um, this is more than 2 orders of magnitude larger than our particle diameter. It is veryimprobable that the particles are crack pinning obstacles. Next, we consider crack deflection as a toughening mechanism. In crack deflection, the crack is tilted and twisted around the particles, which, causes an increase in the fracture surface area and crack growth occurs in mixed mode fracture (mode I and mode II).39,45 The particles are likely too small to cause this effect. According to Evans et al., the particles need to be larger than the plastic zone radius in order for this mechanism to apply.45,46 To calculate plastic zone radius r_y the following equation was used:

$$r_y = \frac{1}{6\pi}\left(\frac{K_{1c}}{\sigma_y}\right)^2 \quad (2)$$

Where r_y=24.5 mm. The particle diameter is a factor of 1000 smaller than this indicating that crack deflection is not likely for these fillers. Shear band- ing is another common toughening mechanism forparticle filled composites. There was no obvious necking of the sample or evidence of 45° bands in the DIC data or fracture surface. Suggesting there is nosignificantshearbandinginthesesamples. The final mechanism to consider is plastic void growth. This mechanism starts with particle debonding from the matrix and is followed bygrowth of voids. The void growth is the dominant energydissipationmechanism.Tomodelthisthefollowing equations were used: [37]

$$\Delta G_{comp} = \Delta G_m + \Delta G_v \quad (3)$$

$$\Delta G_v = \left(1 - \frac{\nu_m^2}{3}\right)\left(V_v - V_f\right)\sigma_{yc} r_y K_{vm}^2 \quad (4)$$

where ΔG_{comp} is the strain energy release rate of composite, ΔG_m is the strain energy release rate of thematrix,ΔG_vistheenergydissipatedfromplastic voidgrowth,$\nu_m$isvonMisespressuresensitivity,$V_v$is void volume fraction, V_f is filler volume fraction, σ_{yc} is compressive yield stress, and K_{vm} is the von Mises stress concentration factor. The properties used in this calculation are shown in Table 3.[38,47,48]Instead of strain energy release rate, we used the strainenergydensity,areaunderstress–straincurve, forcomposite(U_c)andmatrix(U_m),U_c/U_m=2.6.We assumed that this strain energy density ratio isequal to the strain energy release rate ratio: $\Delta G_{comp}/\Delta G_m$ ratio. A maximum ΔG_v was calculated by assuming all the particles debonded and knowing the average void diameter is 50 nm (Fig 6c). Thecalculation found $\Delta G_v/\Delta G_m$>1.6 indicating 100% particle debonding is an over estimate. Partial particle debonding followed by plastic void growth is the best explanation for the high strain energy density seen in the 200k_0.5 composite.

Conclusions

The result of spliced chain conformation on bulk mechanical properties of SiO_2–PS composites was verified by means of tensile analysis with DIC. Two composite systems were used: one withN ~ P and N>P. For N~P *the* spliced manacles are predictable to be swollen and rise the composite strength, although when $N < P$ the spliced chains are expected to be collapsed and ease particle pull- out. The composites with $N \sim P$ had roughly Constant strength with particle loading and even greater strength than 200k_5.5. The $N < P$ composite had high fracture strain and strength at low loadings, which recommends greater toughness. Toughness assessed with strain energy density for composite 200k_0.5 was double as big as 200k matrix.

SEM images of fracture surfaces recommended that the big strain energy density was due to particle debonding followed by plastic void growing. The high magnification images showed two zones: 1 a sluggish crack growth zone comprising a lot of distortion and huge voids and 2 a fast crack growth zone with fewer distortion and lesser voids. The bulk mechanical properties of polymer Nano composites were systematically studied, it was found that composite P/*N ratio* can be adjusted to raise strength or strain energydensity.

References

1. Shah D, Maiti P, Jiang DD, et al. Effect of nanoparticle mobility on toughness of polymer nanocomposites. Adv Mater.2005;17:525–528.
2. Zhang H, Zhang Z, Friedrich K, et al. Property improvements of in situ epoxy nanocomposites with reduced interparticle distance at high nanosilica content. Acta Mater.2006;54:1833–1842.
3. Wetzel B, Haupert F, Zhang MQ. Epoxy nanocomposites with high mechanical and tribologicalperformance. Compos Sci Technol.2003;63:2055–2067.
4. Zhao X, Zhang Q, Chen D, et al. Enhanced mechanical properties of graphene-based polyvinyl alco- hol composites. Macromolecules. 2010;43: 2357–2363.
5. Dang A, Ojha S, Hui CM, et al. High-transparency polymer nanocomposites enabled by polymer-graft modification of particle fillers. Langmuir. 2014;30: 14434–14442.
6. Kim J, Yang H, Green PF. Tailoring the refractive indices of thin film polymer metallic nanoparticle nanocomposites.Langmuir.2012;28:9735–9741.
7. Zhu J, Uhl FM, Morgan AB, et al. Studies on the mechanism by which the formation of nanocomposites enhances thermal stability. Chem Mater. 2001; 13:4649–4654.
8. Wen X, Wang Y, Gong J, et al. Thermal and flammability properties ofpolypropylene/carbon black nanocomposites. Polym Degrad Stab. 2012;97: 793–801.
9. Gilman J. Flammability and thermal stability studies of polymer layered-silicate (clay) nanocomposites. Appl Clay Sci.1999;15:31–49.
10. Wang J, Dai J, Yarlagadda T. Carbon nanotube - conducting-polymer composite nanowires. Langmuir.2005;21:9–12.
11. Geng Y, Liu MY, Li J, et al. Effects of surfactant treatment on mechanical and electrical properties of CNT/epoxy nanocomposites. Compos Part A: ApplSci Manuf.2008;39:1876–1883.
12. GómezH,RamMK,AlviF,etal.Graphene-con-ducting polymer nanocomposite as novel electrode for supercapacitors. J Power Sources. 2011;196: 4102–4108.
13. Chevigny C, Dalmas F, Di Cola E, et al. Polymer- grafted-nanoparticles nanocomposites: dispersion, grafted chain conformation, and rheological behavior. Macromolecules.2011;44:122–133.
14. Akcora P, Kumar SK, Moll J, et al. Gel-like mechanical reinforcement in polymer nanocompositemelts. Macromolecules.2010;43:1003–1010.
15. Moll JF, Akcora P, Rungta A, et al. Mechanical reinforcement in polymer melts filled with polymer grafted nanoparticles. Macromolecules. 2011;44: 7473–7477.
16. Akcora P, Liu H, Kumar SK, et al. Anisotropic self- assembly of sphericalpolymer-grafted nanoparticles.Nat Mater.2009; 8:354–359.
17. Natarajan B, Neely T, Rungta A, et al. Thermomechanical properties of bimodal brush

modified nanoparticle composites. Macromolecules.2013;46:4909–4918.
18. Ash BJ, Rogers DF, Wiegand CJ, et al. Mechanical properties of Al_2O_3/polymethylmethacrylatenano-composites. Polym Compos.2002;23:1014–1025.
19. Ciprai D, Jacob K, Tannenbaum R. Characterization of polymer nanocomposite interphase and its impact on mechanical properties. Macromolecules.2006;39:6565–6573.
20. Guth E. Theory of filler reinforcement. J ApplPhys.1945;16:20–25.
21. Halpin JC, Kardos JL. The Halpin-Tsai equations: areview. PolymEng Sci.1976;16:344–352.
22. Vaziri H, Abadyan M, Nouri M, et al. Investigation of the fracture mechanism and mechanical proper- ties of polystyrene/silica nanocomposite in varioussilica contents. J Mater Sci.2011;46:5628–5638.
23. Li Y, Krentz TM, Wang L, et al. Ligand engineering of polymer nanocomposites: from the simple to the complex. ACS Appl Mater Interfaces. 2014;6: 6005–6021.
24. Li Y, Tao P, Viswanath A, et al. Bimodal surface ligand engineering: the key to tunable nanocompo- sites. Langmuir.2013;29:1211–1220.
25. Zheng Y, Abbas ZM, Sarkar A, et al. Surface-initi- ated reversible addition-fragmentation chain trans- fer polymerization of chloroprene and mechanical properties of matrix-free polychloroprenenanocom-posites. Polymer.2018;135:193–199.
26. Donald AM, Kramer EJ. Effect of molecular entan- glements on craze microstructure in glassy poly-mers. J PolymSciPolymPhys Ed.1982;20:899–909.
27. Kramer EJ, Berger LL. Fundamental processes of craze growth and fracture. In: H.-H. Kausch, editor. Crazing in polymer. Berlin, Heidelberg: Springer; 1990.
28. Matsen MW, Gardiner JM. Autophobicdewetting of homopolymer on a brush and entropic attraction between opposing brushes in a homopolymer matrix. J Chem Phys.2001;115:2794–2804.
29. Trombly DM, Ganesan V. Curvature effects uponinteractions of polymer-grafted nanoparticles in chemically identical polymer matrices. J ChemPhys.. 2010;133:154904
30. Meng D, Kumar SK, Ge T, et al. Crazing of nanocomposites with polymer-tethered nanopar-ticles. J Chem Phys.2016;145:094902
31. Hassinger I, Li X, Zhao H, et al. Toward the development of a quantitative tool for predicting dispersion of nanocomposites under non-equilib- rium processing conditions. J Mater Sci. 2016;51: 4238–4249.
32. Zhang Y, Zhao H, Hassinger I, et al. Microstructure reconstruction and structural equation modeling for computationaldesignof nanodielectrics. IntegrMater ManufInnov. 2015;4:14.
33. Xu H, Li Y, Brinson C, et al. A descriptor-based design methodology for developing heterogeneous microstructural materials system. J Mech Des. 2014; 136:051007.
34. Schreier H, Orteu J-J, Sutton MA. Image correlation for shape, motion and deformation measurements. Boston, MA: Springer US;2009.
35. Chevigny C, Jestin J, Gigmes D, et al. Wet-to-dry conformational transition of polymer layers grafted to nanoparticles in nanocomposite. Macromolecules.2010;43:4833–4837.
36. Eriksson M, Goossens H, Peijs T. Influence of dry- ing procedure on glass transition temperature of PMMA based nanocomposites. Nanocomposites. 2015;1:36–45.
37. Johnsen BB, Kinloch AJ, Mohammed RD, et al. Toughening mechanisms of nanoparticle-modified epoxy polymers. Polymer.2007;48:530–541.
38. Huang Y, Kinloch AJ. Modelling of the toughening mechanisms in rubber-modified epoxy polymers part II: a quantitative description of the microstruc- ture-fracture property

relationships. J Mater Sci. 1992;27:2763–2769.
39. Huang Y, Kinloch AJ. Modelling of the toughening mechanisms in rubber-modified epoxy polymers part 1: finite element analysis studies. J Mater Sci. 1992;27:2753–2762.
40. Lange FF. The interaction of a crack front with asecond-phase dispersion. Philos Mag. 1970;22: 983–992.
41. Green D, Nicholson P, Embury J. Fracture of a brit- tle particulate composite, part 2: theoretical aspects. J Mater Sci.1979;14:1657–1661.
42. Kinloch AJ, Maxwell DL, Young RJ. The fracture of hybrid-particulate composites. J Mater Sci. 1985;20: 4169–4184.
43. Lange FF, Radford KC. Fracture energy of an epoxy composite system. J Mater Sci.1971;6:1197–1203.
44. Kinloch AJ, Young RJ. Fracture behaviour of poly- mers. New York: Applied Science Publishers;1983.
45. Evans AG, Williams S, Beaumont PWR. On the toughness of particulate filled polymers. J Mater Sci. 1985;20:3668–3674.
46. Evans AG. The strength of brittle materials contain- ing second phase dispersions. Philos Mag. 1972;26: 1327–1344.
47. S. Lampman, editor. Characterization and failure analysis of plastics. Singapore: ASM International; 2003.
48. Wu JJ, Buckley CP. Plastic deformation of glassy polystyrene: a unified model of yield and the role of chain length. J PolymSci B: Polym Phys. 2004; 42: 2027–2040.